High-speed escape jumps in haptophytes: Mechanism and triggering fluid signal

Miano, Federica; Asadzadeh, Seyed Saeed; Ryderheim, Fredrik; Andersen, Anders; Kiørboe, Thomas

Published in:
Limnology and Oceanography

Link to article, DOI:
10.1002/lno.12713

Publication date:
2024

Document Version
Publisher's PDF, also known as Version of record

LIMNOLOGY and OCEANOGRAPHY

ASLO

Limnol. Oceanogr. 69, 2024, 2846–2858

doi: 10.1002/lno.12713

High-speed escape jumps in haptophytes: Mechanism and triggering fluid signal

Federica Miano,[1*] **Seyed Saeed Asadzadeh**,[1] **Fredrik Ryderheim**,[1,2] **Anders Andersen**,[1] **Thomas Kiørboe**[1]

[1]Centre for Ocean Life, National Institute of Aquatic Resources, Technical University of Denmark, Kongens Lyngby, Denmark
[2]Marine Biological Section, Department of Biology, University of Copenhagen, Helsingør, Denmark

Abstract

Some planktonic organisms can remotely sense and evade predators by powerful escape jumps. Remote perception typically happens through the fluid disturbance generated by the approaching predator or its feeding current. In copepods and ciliates with mechanosensors, the perception and jump mechanisms are well understood. But how some flagellates perceive the fluid disturbance and achieve similar relative speeds with only two flagella is less explored. Here, we examined the ability of three haptophytes, *Chrysochromulina simplex*, *Prymnesium polylepis*, and *Prymnesium parvum*, to sense and evade the fluid disturbance generated by the feeding current of a copepod nauplius. *Chrysochromulina simplex* has a long haptonema (14 cell diameters), while the haptonema of the two other species are shorter (1 and 0.5 cell diameters). Only *C. simplex* responded to the fluid disturbance by fleeing at high speeds. The jump mechanism consists of two phases: the rapid coiling of the haptonema that pulls the cell about two cell diameters in the direction of the haptonema, followed by flagellar reversal and high-speed swimming (70 cell lengths per second) in the opposite direction. We rationalize cell displacements and escape speeds from haptonema and flagellar kinematics and fluid dynamics. Using a microfluidic channel, we demonstrate that the component of the fluid signal that triggers the jumps is the maximum deformation rate rather than the magnitude of deformation. High-speed escape jumps may be an avoidance mechanism evolved by haptophytes with long and coiling haptonema, while species with shorter haptonema may use other defense mechanisms, such as stealth and toxicity.

Unicellular flagellates occupy a key position in marine food webs as important primary producers and as the main grazers of bacteria and other picoplankton (Calbet and Landry 2004). At the same time, they are grazed by zooplankton and hence transfer primary production to higher trophic levels (Fenchel 1982). Thus, they are both consumers and prey, and their success in the food web is determined by the trade-off between resource acquisition and predator avoidance.

Protists have developed different predator avoidance strategies to increase the chance of survival. Some have "stealth" behavior and thus minimize predator encounter rates, typically at the cost of lower foraging efficiency (Nielsen and Kiørboe 2021). Others have evolved more explicit strategies like production of grazer deterrent toxins, bioluminescent flashes, or change in size or colony formation in response to grazer cues to reduce grazing mortality (Pančić and Kiørboe 2018; Lürling 2021). Finally, some protists can remotely perceive and evade predators by powerful escape jumps (Jakobsen 2001; Jakobsen 2002; Jakobsen et al. 2006). Remote perception of predators in the plankton typically happens through fluid disturbances and it is often assumed—and sometimes demonstrated—that it is the maximum deformation rate generated by the approaching predator or its feeding current that the prey perceives (Kiørboe and Visser 1999; Kiørboe 2008). While the perception mechanism is well understood in copepods that are equipped with mechanosensory hairs (Kiørboe and Visser 1999; Shen et al. 2020, Shen et al. 2021), it is less clear how single-celled protists can perceive

*Correspondence: fmia@aqua.dtu.dk

Additional Supporting Information may be found in the online version of this article.

Author Contribution Statement: FM and TK conceived the study. FM gathered the data with assistance from FR for the predator experiment. FM analyzed the data with assistance from SSA and TK for interpretation of the results and FR for statistical analyses. FM, AA, and SSA developed the fluid dynamical models of the jump mechanism. SSA developed and carried out the computational fluid dynamics simulation of the microfluidic experiment. FM wrote the first draft of the manuscript with contributions from TK. All authors reviewed and approved the final version of the manuscript.

predator-generated fluid disturbances, and what component of the fluid disturbance is perceived (Jakobsen 2002). The ciliate *Mesodinium rubrum* has long cirri (bundles of cilia) that extend 1–2 cell diameters into the surrounding water, and they supposedly function as mechanosensors (Fenchel and Hansen 2006). Bioluminescent flashes in dinoflagellates are elicited in fluid shear (Maldonado and Latz 2007), even though they have no mechanosensory structures extending into the surrounding fluid. Experiments have demonstrated that flashes may be elicited by mechanically deforming cells, and that flashing is governed both by the magnitude and the rate of cell deformation (Jalaal et al. 2020).

Similarly, while the mechanism by which copepods can accelerate to escape speeds of hundreds of body lengths per second has been explained (Buskey et al. 2002; Kiørboe et al. 2010), it is less obvious how protists may achieve similar relative speeds. The ciliate *M. rubrum* has a girdle of membranelles formed by many cilia that enables very high escape speeds (Fenchel and Hansen 2006), and other ciliates have a contractive "tail" that may pull the cell at $\sim$ 1000 body lengths per second during escapes (Gemmell et al. 2015), but how flagellates equipped with only two flagella can achieve similar relative speeds is unknown (Jakobsen 2002; Jakobsen et al. 2006).

Some biflagellated haptophytes are known to both sense fluid signals and escape at high speeds (Jakobsen 2002). Many haptophytes are equipped with a haptonema, a long, slender organelle positioned between the two flagella. The haptonema consists of an endoplasmatic reticulum enclosing three to seven microtubules (Manton and Parke 1962; Manton 1964, 1967). It does not actively beat like a flagellum, but it can bend and coil. In some species, the haptonema is used as a food-capturing device, and like an elephant trunk it can bend and deliver captured prey particles to the "mouth" (Kawachi et al. 1991; Kawachi and Inouye 1995). The haptonema likely plays a role in sensing (fluid) disturbances, and in some species the haptonema can rapidly coil following mechanical stimulation (Nomura et al. 2019).

Here, we examined the ability of three haptophyte species to sense and evade the fluid disturbance generated by a feeding-current feeding predator. The three haptophytes, *Chrysochromulina simplex*, *Prymnesium polylepis*, and *Prymnesium parvum*, possess a haptonema that is much longer than, comparable to, and shorter than the cell body, respectively. We first used high-magnification and high-speed video microscopy to observe the behaviors of freely swimming and jumping haptophyte cells. Then, we observed their behavior when exposed to the fluid disturbance generated by the feeding current of a predator, nauplii of the copepod *Temora longicornis*. Finally, we used a convergent microfluidic channel to mimic the predator-generated flow and examined whether the magnitude of the fluid deformation or the maximum deformation rate, or both, elicited an escape response. For the only jumping species, *Chrysochromulina simplex*, we rationalized the jump mechanism and quantitatively characterized the triggering fluid signal.

Materials and methods

Culturing

Chrysochromulina simplex (strain K-0561, University of Copenhagen), *Prymnesium polylepis* (strain K-0259, University of Copenhagen), and *Prymnesium parvum* (strain K-0081, University of Copenhagen) were grown in L1 medium without silica at 18°C (*C. simplex* and *P. parvum*) or 16°C (*P. polylepis*) at 100 μmol photons m^{-2} s^{-1}. Morphometrics of the cell body and the haptonema were estimated from live images of freely swimming cells, assisted by live and transmission electron microscopic images from the literature (Manton and Parke 1962; Green et al. 1982; Birkhead and Pienaar 1995).

Temora longicornis nauplii in development stages 3 and 4 (200–250 μm) were obtained from our continuous laboratory culture maintained at 18°C on a mixture of flagellates and diatoms as food.

Freely swimming cells

We video recorded the behavior of individual freely swimming cells inside a chamber consisting of a plastic ring (16 mm inner diameter and 3 mm height) fixed with Vaseline® on a coverslip and sealed on top with a second coverslip. Occasionally, cells performed escape jumps, for example, as they bumped into one another, allowing us to observe both routine swimming and escapes. The recordings were carried out with an Olympus IX71 inverted microscope equipped with a Phantom Miro LAB 320 high-speed video camera (1920 $\times$ 1200 pixels), using an Olympus LCPlanFl objective $\times$40/0.60, an Olympus UPlanSApo oil immersion objective $\times$100/1.40, and an Olympus UPLanFL N oil immersion $\times$100/1.30 objective for phase-contrast imaging. The frame rate ranged from 500 to 1500 frames s^{-1}. The image analysis software ImageJ (Fiji) was used for morphometrics, speed, and flagellar beat frequency measurements, and for detailed observations of flagellar beating patterns and haptonema configurations. All distances were measured as two-dimensional projections and were therefore conservative. The observations were made in a temperature-controlled room at 20°C. To avoid overheating the sample under the microscope light, the exposure time was limited to 10 min.

Fluid signals

We examined two components of the fluid disturbance, namely the magnitude of deformation, ϵ, and the maximum deformation rate, Δ. The magnitude of deformation, ϵ, is the total fluid deformation experienced by the flagellate between the start of the convergent section of the microfluidic channel and the initial escape position, due to increasing fluid velocity along the convergent section. If we follow a fluid element, we can define the magnitude of deformation as the ratio between

the length of the fluid element at the initial escape position and at the start of the convergent section. Therefore, the magnitude of deformation can be calculated as:

$$\epsilon = \frac{u_J}{u_1} \quad (1)$$

where u_J and u_1 are the fluid velocity at the initial escape position and at the start of the convergent section, respectively. *See* Eq. 5 in Supporting Information for the final expression used for the calculation of the magnitude of deformation ϵ.

The maximum deformation rate, Δ, is the rate of fluid deformation in the direction that yields the maximum deformation, that is, the direction in which the fluid element is elongated or compressed the most. Following (Kiørboe and Visser 1999), it can be calculated as the maximum of the absolute values of λ_1, λ_2, and λ_3:

$$\Delta = \max\{|\lambda_1|, |\lambda_2|, |\lambda_3|\} \quad (2)$$

where λ_1, λ_2, and λ_3 are the eigenvalues of the rate-of-strain tensor of the fluid velocity field (*see* Eq. 6 in Supporting Information).

Behavior in the feeding current of a predator

Individual nauplii were glued to a human hair by their dorsal surface using cyanoacrylate-based super glue. The hair was then attached to a micromanipulator and the tethered nauplius was submerged in a $10 \times 10 \times 10\ \text{cm}^3$ aquarium filled with filtered seawater. The nauplii beat their feeding appendages at approximately 30 Hz to produce a feeding current (Bruno et al. 2012). Suspensions of haptophytes and 6.2-μm latex beads were added before observations started. The beads were previously treated with surfactant by dissolving $1\ \text{mg mL}^{-1}$ of bovine serum albumin into the bead solution and then sonicating it until no agglomeration was observed. Foraging sequences were recorded at 500 frames s^{-1} using a Phantom V210 high-speed camera (Vision Research First) equipped with lenses to provide a field of view of $1.3 \times 1.0\ \text{mm}^2$. Collimated infrared light was provided by a lamp shining through the aquarium directly toward the camera.

We used ImageJ to track tracer particles to determine the feeding current. Particles were tracked at a lower frequency (25 Hz) than the recording frequency due to the noise generated by the movement of the nauplii appendages. We selected particles that remained in the focal plane and tracked them until they reached approximately 100 μm from a reference point located at the middle of the nauplius. The motion of particles closer to the nauplius was highly fluctuating due to appendages movement. We estimated the particle speed as particle displacement over time.

Only *C. simplex* showed behavioral changes in response to the fluid disturbance generated by the feeding current. Cells that entered the feeding current were easily recognizable as they moved along the flow streamlines with increasing speed as they approached the predator. We identified 50 escape jumps as cells that changed swimming direction between two time frames, thus deviating from the trajectory imposed by the flow. We estimated the maximum deformation rate of the fluid flow at the initial escape positions using the jumping cells as tracers. For each jumping cell, we tracked it backward and determined its speed from the moment it entered the feeding current up to the visible deviation. We considered the largest value of the spatial derivative of the cell speed in this interval as a conservative estimate of the maximum deformation rate of the fluid flow. The initial escape position was identified as the point along the cell trajectory corresponding to the largest value of the spatial derivative of the cell speed. For each escape jump, we collected the initial escape positions and the corresponding maximum deformation rates, Δ, and looked at the relative frequency distribution of Δ in log-scaled bins and its geometrical mean, since the Δ values were near log-normally distributed.

Microfluidic channel

We used a microfluidic channel to further characterize the fluid signal that triggers escapes. The channel was fabricated from polydimethylsiloxane with the standard SU8 molding method. The mold was fabricated using an epoxy-based negative photoresist (NANO™ SU-82000 by MICROCHEM). To achieve the desired geometry on the mold, the photoresist film was exposed to UV light using a laser writer (LPKF ProtoLaser LDI). The channel had a rectangular cross-section of constant height, $h = 0.28$ mm, and variable width: a broad, upstream section of constant width $W_1 = 1.15$ mm, a narrow, downstream section of constant width $W_3 = 0.23$ mm, and a convergent section of length $L = 0.5$ mm and width:

$$W_2(x) = W_1 + \frac{x}{L}(W_3 - W_1) \quad (3)$$

that connected the upstream and downstream sections (Fig. 1a). The origin of the coordinate system is at the middle of the bottom wall at the entrance to the convergent section, and the coordinate x is in the downstream direction.

The channel is designed to have a convergent section where the cells experience increasing velocity and, hence, fluid deformation as they are carried with the flow. We estimated the spatial distribution of the magnitude of deformation, ϵ, and the maximum deformation rate, Δ, in the convergent section of the channel at the midplane $z = h/2$. The magnitude of deformation, ϵ, was calculated analytically using Eq. 5 in Supporting Information. The maximum deformation rate, Δ, was estimated numerically with computational fluid dynamics (Fig. 1b; Supporting Information). Because the maximum deformation rate at a certain position increases proportionally with the flow rate, while the magnitude of

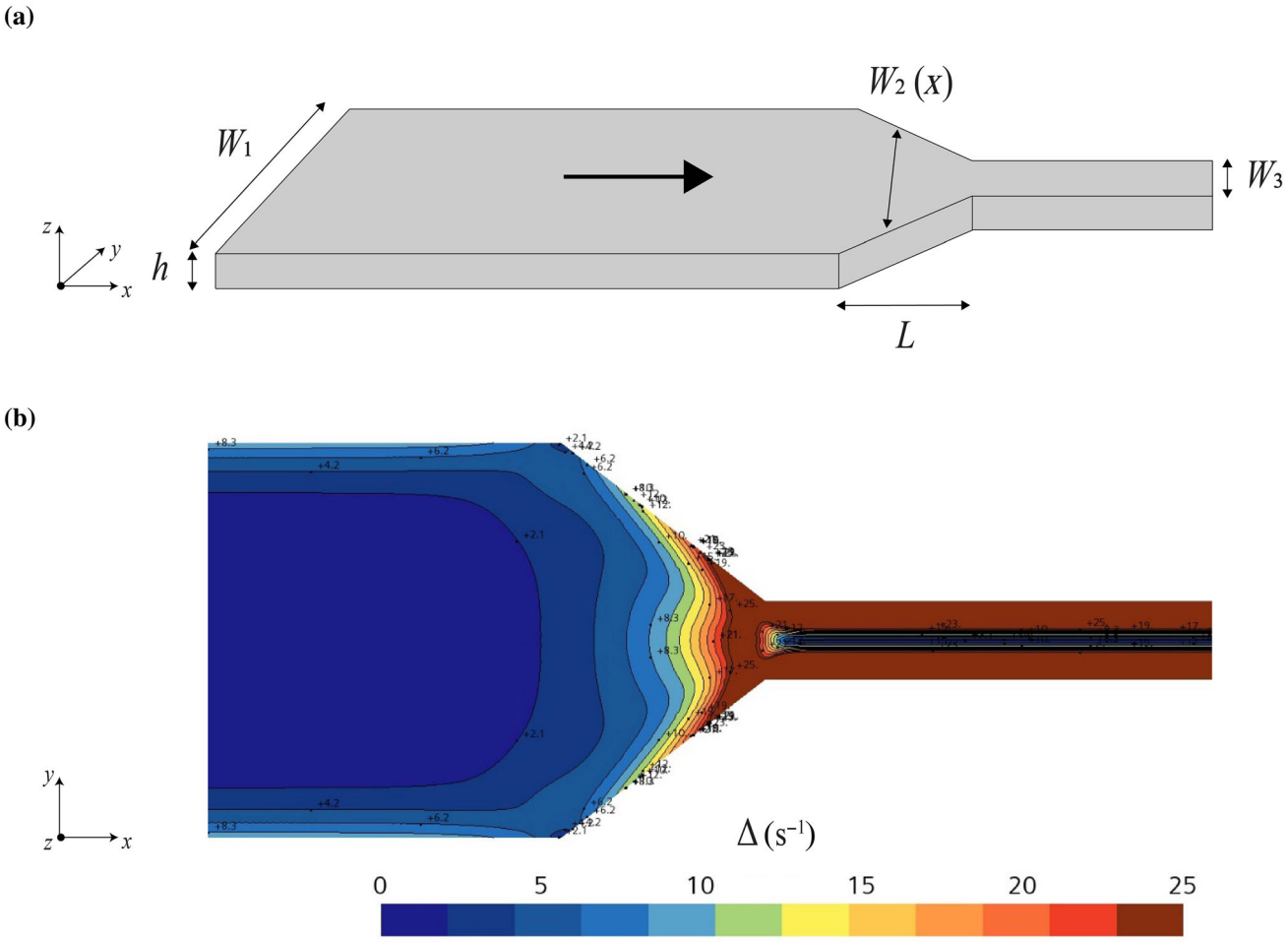

Fig. 1. (**a**) Schematics of the microfluidic channel with the flow in the direction of the thick arrow from left to right. (**b**) The maximum deformation rate, Δ, at the midplane $z = h/2$ for $Q = 20\ \mu$L min^{-1}. All reported escape events were located in the midplane.

deformation is independent of the flow rate, we could separate the effects of the two possible triggering signals by varying the flow rate between experiments.

We made all the observations at the midplane $z = h/2$, where the vertical velocity gradient and hence the vertical component of fluid deformation are both zero. However, the objective used had a focal depth of approximately $\pm$ 15 μm, potentially introducing a z-component in the fluid deformation. Through computational fluid dynamics simulations we verified that for $h = 280\ \mu$m the variation of Δ in the interval $z = \pm 15\ \mu$m from the midplane was small compared to its magnitude (relative difference lower than 20%; *see* Supporting Information Fig. S1). The magnitude of deformation, ϵ, is independent of z.

Microfluidic experiments

Suspensions of the haptophytes were introduced into the microfluidic device, where a steady flow was imposed through a pressure pump equipped with a flow rate controller (LineUp Flow EZ, LINK Module and Flow Unit by FLUIGENT). Experiments were performed at different constant flow rates of 20, 30, 40, and 50 μL min $^{-1}$, to cover the desired range of Δ, 2–30 s^{-1}, as observed in the copepod feeding current, and in the feeding currents of other potential predators (Kiørboe et al. 1999). The behavior of the cells flowing inside the channel was observed through high-speed video microscopy (Olympus IX71 inverted microscope, Phantom Miro LAB 320 camera, Olympus UPlanFl $\times$10/0.30) at frame rates ranging from 300 to 500 frames s^{-1}. All the recordings were made at the midplane $z = h/2$, and the field of view included the convergent section. To make sure that the cells had not been recently exposed to the fluid disturbance, we first filled the chamber with the suspension of cells and stopped the pump for a few minutes before each recording. When reactivating the pump and starting recording, the recording time was kept short to guarantee that it was only cells already in the broad section that entered the convergent section.

As for the predator experiment, we identified escape jumps as cells with trajectories that deviated from the local streamlines. We followed back the cells for 15 ms prior to the visible

deviation to take into account the response latency between sensing of the fluid signal and the motor response. In this way, we identified the initial escape positions and the corresponding values of the magnitude of deformation, ϵ, and the maximum deformation rate, Δ. We identified a total of 143 escape jumps, respectively 32, 36, 37, and 38 at the four operating flow rates. For each flow rate, we looked at the relative frequency distribution of ϵ and Δ in log-scaled bins and their geometrical means, since the ϵ and Δ values were near log-normally distributed.

Statistics

We analyzed how the magnitude of deformation ϵ changed with flow rate using a generalized linear model with a Gaussian family in R version 4.3.2. The maximum deformation rates were analyzed using one-way ANOVA. The maximum deformation rate data were $\log_{10}$-transformed prior to running the analysis to achieve normally distributed residuals. Levene's test was used to test for homogeneity of variance. The models were validated by visual inspection of the residual plots. The statistical tests were considered significant at the 0.05 level and are summarized in Supporting Information Tables S1 and S2.

Results

Freely swimming cells

We identified two different swimming gaits for *C. simplex* and *P. polylepis* and only one for *P. parvum* (Fig. 2).

Chrysochromulina simplex

During routine swimming, the two flagella are extended backward and beat in phase with an undulatory planar beat, propelling the cell slowly forward along a nearly straight trajectory while rotating around an axis parallel to the swimming direction. The long haptonema is pointing in the swimming direction (Fig. 2a; Table 1; Supporting Information Video S1).

When disturbed, for example following mechanical stimulation, the cell initiates escape jumping. First, the haptonema coils while pulling the cell forward (Supporting Information Video S1). The coiling happens very quickly, shortening the long organelle to a stack of coils of approximately the same size as the cell body in a few milliseconds. Coiling begins at the distal half of the haptonema, where the organelle first deforms with gentle helices followed by sequential coiling from the tip (Fig. 3a). During the first part of the coiling, the cell is pulled forward in the direction of haptonema at very high speed (frames sequence 0–2.8 ms; Fig. 3a–c; Table 1), but this is counteracted during the second half of the coiling by reversal of the flagella, which are moved from behind to the side of the cell body (frames sequence 3.5–11.4 ms; Fig. 3a). Subsequently, the cell reversed its swimming direction and accelerated to a speed nearly two orders of magnitude higher than undisturbed swimming, while increasing the flagellar beat frequency 30-fold (Fig. 3b,c; Table 1; Supporting Information Video S1). During the reversed swimming phase, the flagella beat on the sides of the cell body almost completely out of phase in a three-dimensional pattern characterized by power and return strokes (Fig. 2b; Table 1; Supporting Information Video S1). The cell followed a three-dimensional trajectory while rotating around itself in a tumbling fashion, carrying the coiled haptonema underneath the cell body (Supporting Information Video S1).

After some time, which exceeds the time the cell is in the field of view (approximately 0.5 s), the flagella slow down, the cell stops, and the haptonema slowly uncoils within approximately 2 s (Supporting Information Video S1). Once the haptonema was completely extended again, the flagella switched to their original configuration and the cell returned to routine swimming.

There is a response latency of approximately 15 ms between the onset of the mechanical stimulus and the actual escape from the stimulus, when the cell initiates high-speed, reversed swimming. The response latency is determined as the sum of the time-lag between the stimulus and the initial contraction of the haptonema of 2–3 ms (Supporting Information Video S2) and the time-lag between the initial contraction and the initiation of reversed swimming of 12–13 ms (Fig. 3a,c; Supporting Information Video S2).

Prymnesium polylepis

During routine swimming, the two flagella are extended backward and beat in phase with an undulatory planar beat, as previously described by Dölger et al. (2017). *Prymnesium polylepis* swim as *C. simplex* with a nearly straight trajectory with the haptonema pointing forward and the cell rotating around the axis corresponding to its swimming direction, but *P. polylepis* swim at higher speed than *C. simplex* due to the higher flagellar beat frequency and the smaller drag on the shorter haptonema (Fig. 2c; Table 1; Supporting Information Video S3).

When disturbed, the cell slowly changes swimming direction by changing the flagellar configuration. One flagellum increases its beat frequency while quickly moving to a new position, and the other one slows down drastically and almost stops beating. This asymmetry makes the cell rotate toward the slow flagellum and thus change swimming direction. Sometimes, the cell can reverse both flagella and swim backward for a while. While changing swimming direction, the flagella keep the same undulatory planar beat, the haptonema remains extended, and the swimming speed is slightly reduced. When the maneuver is completed, the flagella turn back to the original position and the cell continues swimming in the new direction (Fig. 2d; Table 1; Supporting Information Video S3).

Prymnesium parvum

During routine swimming, the two flagella beat on the side of the cell body almost completely out of phase with a three-

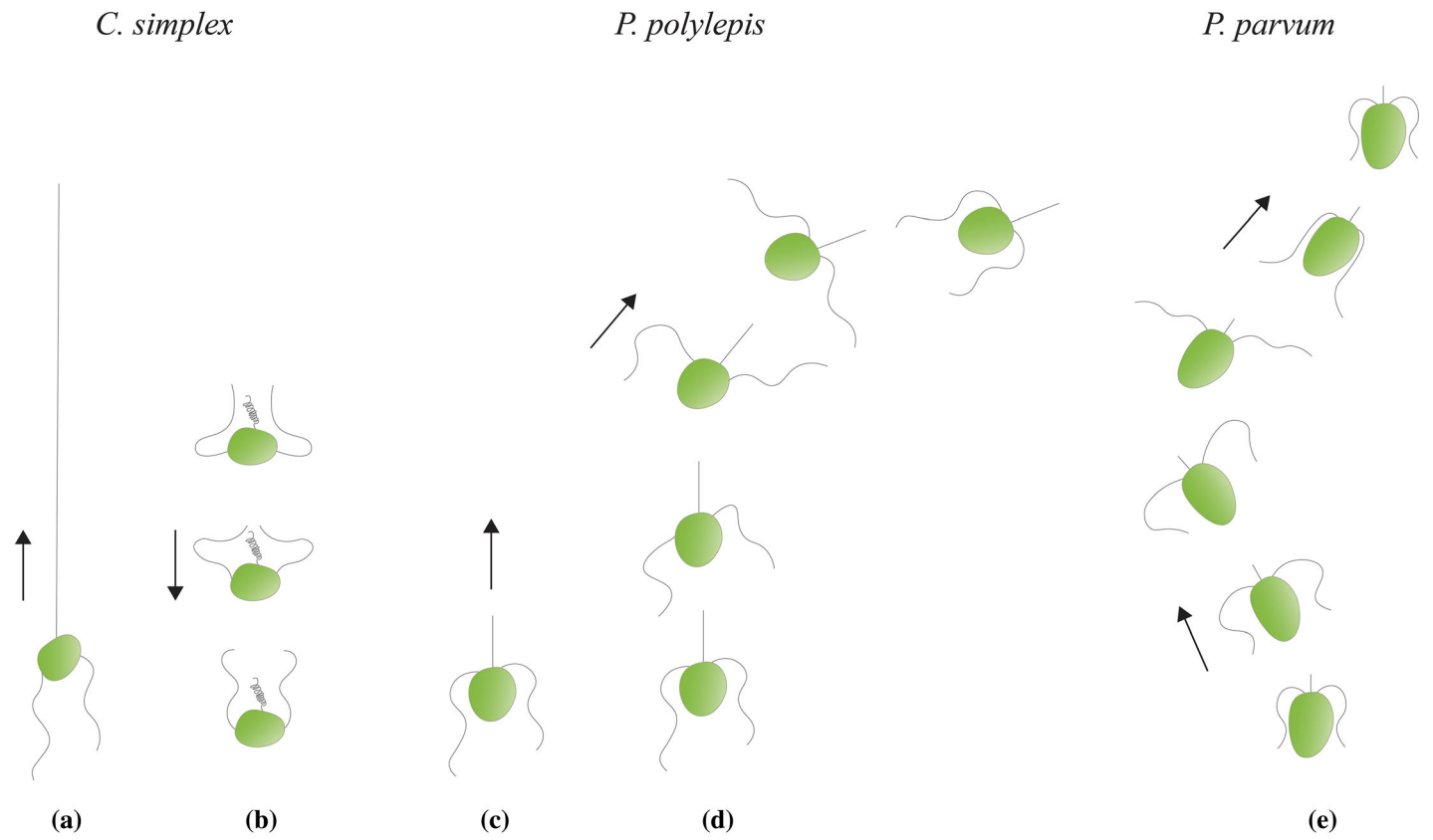

Fig. 2. Schematics of the swimming gaits observed in the three species. (**a**) *Chrysochromulina simplex* undisturbed swimming and (**b**) escape jumping in response to disturbance. (**c**) *Prymnesium polylepis* undisturbed swimming and (**d**) response to disturbance. (**e**) *Prymnesium parvum* undisturbed swimming. Black arrows indicate directions of motion.

dimensional beat pattern characterized by power and return strokes. The cell swims in a tumbling fashion along a three-dimensional trajectory with the haptonema pointing forward (Fig. 2e; Table 1; Supporting Information Video S4). The cells do not show any behavioral changes in response to disturbances, for example, when bumping into each other.

Exposure to predator feeding current

When exposed to the feeding current of the nauplius of *T. longicornis*, only *C. simplex* showed behavioral changes. Several cells were entrained by the feeding current that accelerates toward the nauplius, and the cells were able to escape through powerful jumps once they reached a critical distance from the

Table 1. Morphometrics, beat frequencies, and swimming speeds for the three haptophytes in the free-swimming configuration, and in the escape configuration for *Chrysochromulina simplex*. Average ± standard deviation; number of observations in parentheses. The beat frequencies have been measured separately on both flagella, and then averaged.

			Flagellar beat frequency (Hz)		Swimming speed (μm s^{-1})		Cell displacement during coiling	
	Cell width (μm)	Haptonema length (μm)	Routine	Disturbed	Routine	Disturbed	Distance (μm)	Speed (μm s^{-1})
C. simplex (K-0561)	4.7 ± 0.7 (15)	65 ± 13 (10)	5 ± 3 (9)	145 ± 11 (5)	5 ± 2 (7)	316 ± 73 (5)	6.9 ± 2.7 (5)	1747 ± 424 (5)
Prymnesium polylepis (K-0259)	7.3 ± 1.3 (10)	9.2 ± 1.2 (10)	80 ± 22 (6)	125 ± 4* (4)	53 ± 29 (6)	47 ± 23 (3)		-
Prymnesium parvum (K-0081)	6.4 ± 1.0 (3)	3.2 ± 0.3 (3)	45 ± 6 (2)	-	45 ± 3 (2)	-		-

*The beat frequency of the fast flagellum; the other flagellum slows down drastically, and it almost stops beating while the cell is rotating.

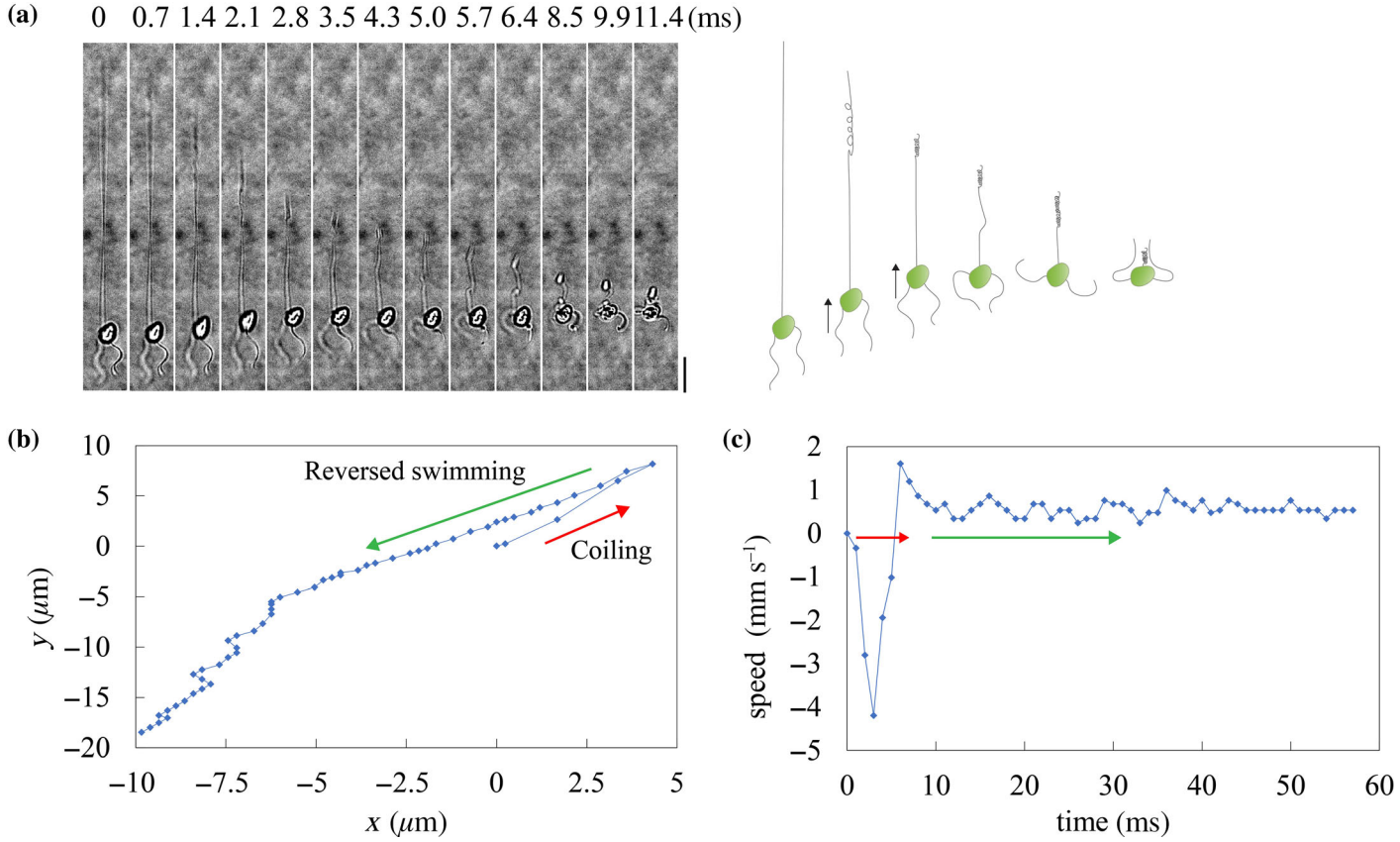

Fig. 3. Escape jumping in *Chrysochromulina simplex*. (**a**) Frame sequence and schematics of the haptonema coiling and flagella reversal, before initiating reversed swimming (Fig. 2b). Scale bar: 10 μm. (**b**) Tracking and (**c**) velocity of a jumping cell during the two phases of the escape jump, haptonema coiling and reversed swimming.

nauplius (Supporting Information Video S5). Depending on the initial escape position, some cells were able to successfully swim away from the predator, while others were trapped again in the feeding current after the escape jump was terminated. Generally, jumps that initiated close to the nauplius, specifically within the x and y coordinates range of (−200, 200) μm (Fig. 4a), did not result in successful escapes. However, several cells were eventually able to initiate another escape jump, after the first one terminated.

The escape positions of *C. simplex* are concentrated in the feeding current region, especially where the flow speed is increasing rapidly (longer distances between tracer particle positions) (Fig. 4a). The few escape reactions far from the copepod are likely due to cells bumping into one another. The frequency distribution of the maximum deformation rate Δ experienced by the cells at the initial escape positions is near log-normally distributed with a geometrical mean of 13.5 s^{-1} (Fig. 4b).

Microfluidic channel

As with the copepod feeding current, only *C. simplex* showed behavioral responses to the flow in the microfluidic channel (Supporting Information Video S6). The spatial distribution of escape jumps in the convergent section of the channel moves toward the broad section with increasing flow rates (Supporting Information Fig. S2). The frequency distributions of the magnitude of deformation, ϵ, and the maximum deformation rate, Δ, at the initial escape positions at the four operating flow rates respectively, are near log-normally distributed (Fig. 5). The magnitude of deformation at the escape positions was highest at the flow rate 20 μL min^{-1}, and it decreased significantly as the flow rate increased (generalized linear model, slope = -0.033 ± 0.005, $t = -7.373$, $p \leq 0.0001$) (Fig. 5a; Table 2; Supporting Information Table S1). Conversely, there was no effect of the flow rate on Δ at the escape positions (ANOVA, $F_{3,139} = 0.129$, $p = 0.943$) (Fig. 5b; Table 2; Supporting Information Table S2).

Discussion

Among the three species examined, *C. simplex* showed two swimming gaits in the observation chamber and responded to the fluid disturbance generated by both the predator feeding current and the microfluidic channel flow by powerful escape jumps (second swimming gait). *Prymnesium polylepis* also showed two swimming gaits, but it did not respond to the fluid disturbance in either the predator or the microfluidic

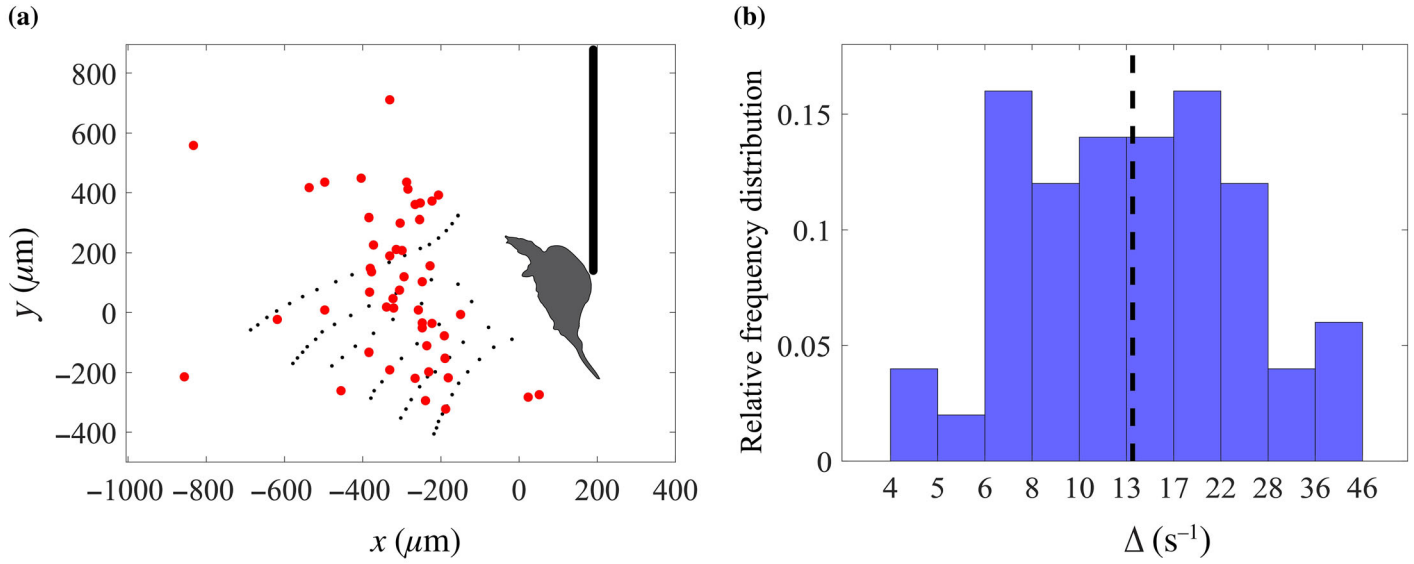

Fig. 4. (**a**) The nauplius *Temora longicornis* with its feeding current visualized by tracks of tracer particles with 0.125 s between the displayed black dots, and escape positions of *Chrysochromulina simplex* (red dots). Escapes are plotted in a coordinate system with origin in the middle of the copepod. (**b**) Relative frequency distribution of the maximum deformation rate, Δ, at the initial escape positions and its geometrical mean of 13.5 s^{-1} with 95% confidence interval (10.6–17.1) s^{-1} (dashed line). Number of observations: 50. The escape positions are corrected for response latency.

experiment. The second swimming gait consisted of asymmetric beating of the two flagella, which resulted in changes of the swimming direction without acceleration, much the same way as it has been described in other biflagellates (Polin et al. 2009; Wan et al. 2014). This gait was not observed in response to the fluid disturbance and might be a response to other types of disturbances, for example, chemical or light. *Prymnesium parvum* showed only one swimming gait, and as expected did not respond to the fluid disturbance in both experiments. Below we first rationalize the escape jump mechanism, and the speeds achieved by *C. simplex* with simple fluid dynamic considerations. We next characterize the fluid signal that elicits an escape response, and we finally discuss the ecological significance and adaptive value of the escape responses found in some protists.

Escape jump mechanism

The escape jump of *C. simplex* can be divided into two phases, each with characteristic elevated speeds: the rapid initial coiling of the haptonema that pulls the cell in the same direction as the swimming direction and typically toward the danger, and the subsequent phase with reversed swimming at high speed (Fig. 3; Table 1).

Haptonema coiling

The coiling process observed in *C. simplex* appears similar to that of *Chrysochromulina* sp. NIES-4122, and it probably has the same motor-independent mechanism regulated by conformational changes of microtubules (Nomura et al. 2019).

During the first half of the haptonema coiling, before the flagella have reversed, the cell is displaced about two cell lengths forward in a few milliseconds, reaching speeds up to 370 body lengths per second (Fig. 3a–c; Table 1). To model the cell displacement of *C. simplex* during the initial phase we consider the force balance on the cell during the first half of the retraction, $D_{H'} = D_C + D_F + D_{H''}$ (Supporting Information Heading 3). The four force terms (D) are the drag on the distal part of the haptonema (H′), the cell body (C), the two flagella (F), and the proximal part of the haptonema (H″) (Supporting Information Fig. S3). The forces scale with the linear dimension and the velocity of the different components. We ignored the thrust force generated by the motion of the flagella in this phase, since their beating is slow relative to the retraction. On these assumptions, we derived an expression for the cell displacement (*see* Eq. 13 in Supporting Information). Using the experimental data in Supporting Information Table S3, the predicted cell displacement was $\Delta r_C = 5.7\,\mu$m, close to the observed 6.9 μm (Table 1).

Among the studied haptophytes, *C. simplex* was the one equipped with the longest haptonema and the only one capable of coiling it. Retraction of nonmotor appendages following mechanical stimulation is common among protists, both in the context of escape and foraging. The ciliates *Pseudotontonia* sp. and *Tontonia* sp. respond to fluid disturbances by rapidly contracting their long "tail" (11x and 5x their cell size, respectively, vs. the 13x in *C. simplex*), pulling the cell 2–4 cell lengths within a few milliseconds at 600–1500 cell lengths per second, typically away from the danger (Gemmell et al. 2015). Subsequently the ciliates continue the escape in the same

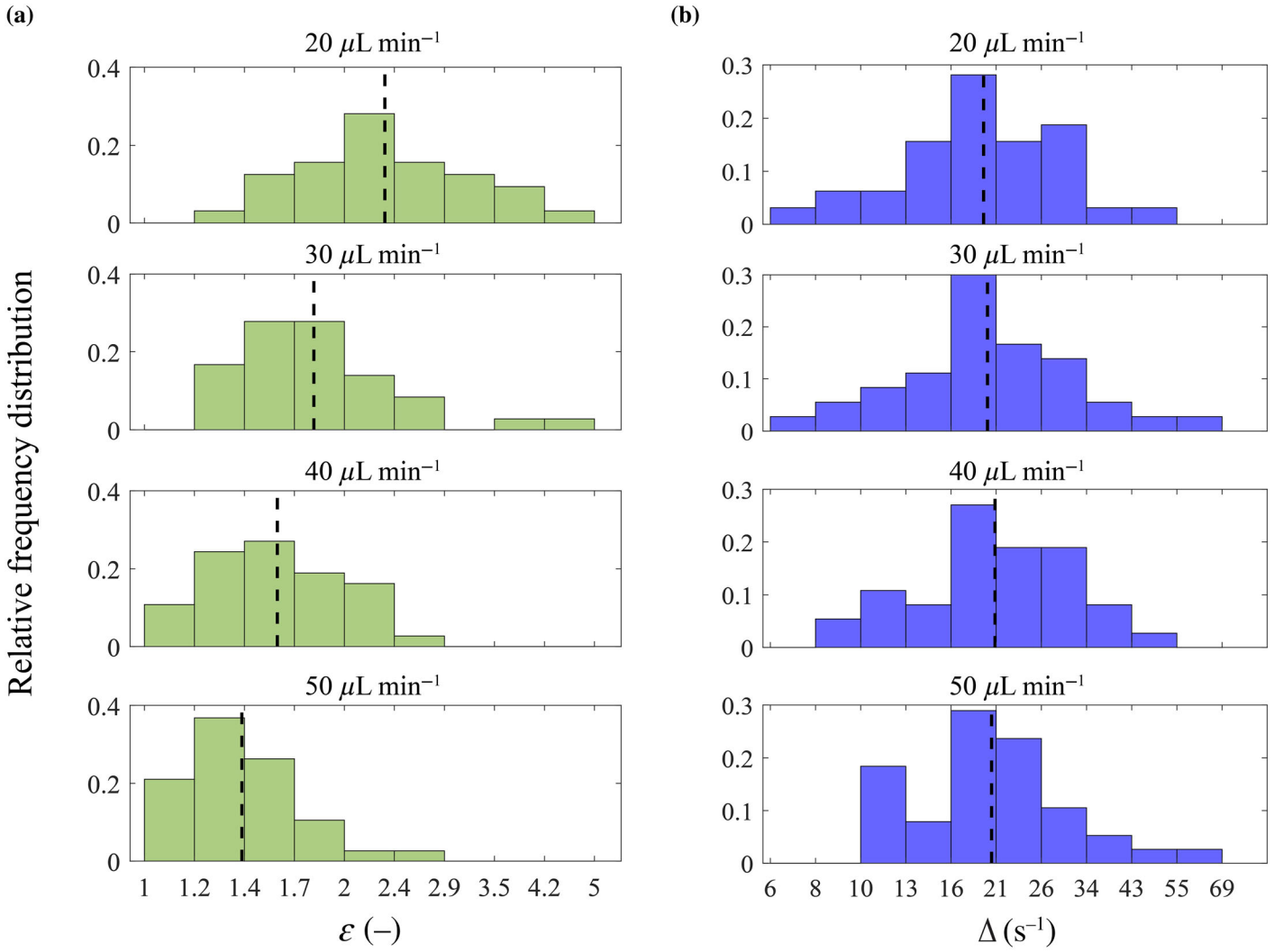

Fig. 5. Frequency distribution of (**a**) the magnitude of deformation, ϵ, and (**b**) the maximum deformation rate, Δ, at the initial escape positions of *Chrysochromulina simplex*, with their geometrical means (dotted lines), at the four different operating flow rates. The escape positions are corrected for response latency.

direction, using the cilia to "push" the organism forward. The sessile ciliate *Vorticella convallaria* can reach speeds of ~ 1200 body lengths per second for threat evasion through the Ca^{2+}-powered rapid coiling of its stalk (spasmoneme) (Ryu et al. 2012). In heliozoan cells, the rapid contraction of needle-like axopodia plays a fundamental role in food capture and ingestion (Ockleford and Tucker 1973; Suzaki et al. 1980, 1992) and it is regulated by extracellular Ca^{2+} concentration (Khan et al. 2003). The haptonema coiling in haptophytes is also dependent on Ca^{2+}, but its microtubule-dependent motility differs from the nonmotor motile systems found in other protists (Nomura et al. 2019).

Table 2. Geometrical means of the magnitude of deformation ϵ and the maximum deformation rate Δ with their 95% confidence interval at the different flow rates.

Flow rate (μL min^{-1})	Number of observations	Magnitude of deformation ϵ (–)	Maximum deformation rate Δ (s^{-1})
20	32	2.4 (2.1–2.7)	19.5 (16.2–22.7)
30	36	1.8 (1.6–2.1)	19.9 (16.0–23.7)
40	37	1.6 (1.5–1.7)	20.7 (17.5–23.9)
50	38	1.4 (1.3–1.5)	20.3 (16.8–23.8)
All	143	1.7 (1.6–1.9)	20.1 (18.4–21.8)

High-speed reversed swimming

After haptonema retraction and reversal of the flagella, the flagella start beating at a frequency 30X higher than during routine swimming, propelling the cell at speeds 63x the routine swimming speed, reaching ~ 70 body lengths per second (Fig. 3c; Table 1) of similar order to that observed by others

(Gregson et al. 1993; Jakobsen 2002). The escape speed of *C. simplex* is about twice that expected from the increased beat frequency. This is due to the reduced drag of the haptonema in the coiled configuration. Using the force balances during routine swimming and escape jumping, and assuming that the thrust forces are proportional to the beat frequencies, we derived an expression for the escape speed (Supporting Information Heading 4):

$$U_{\text{escape}} = \frac{f_{\text{escape}}}{f_{\text{routine}}} \frac{c_S a + c_{t,F} L_F + c_{t,H} L_H}{c_S a + c_{t,F} L_F} U_{\text{routine}} \quad (4)$$

where f_{escape} and f_{routine} are the beat frequencies in the two configurations, a is the radius of the cell body, L_F and L_H are the length of the flagella and the haptonema, respectively, and c_S, $c_{t,F}$, and $c_{t,H}$ are the drag coefficients for the cell body, the flagella, and the haptonema (Supporting Information Heading 3). With the experimental data (Supporting Information Table S3), this yields an escape speed of $U_{\text{escape}} = 306\,\mu\text{m s}^{-1}$, similar to that observed (Table 1). If the haptonema was kept extended during the escape, the second term on the right side of the equation would be equal to unity and the speed of the cell would be halved. Thus, haptonema coiling doubles the escape speed.

Similar relative escape speeds have been observed in protists with much more elaborate flagellar arrangements. Thus, the dinoflagellates *Heterocapsa rotundata* and *Gymnodinium simplex* with very long flagella may escape at speeds of 65 and 98 body lengths per second, (Jakobsen et al. 2006), and the ciliates with many cilia *Mesodinium pulex*, *Strobilidium* sp., *Strobilidium velox*, and *Halteria grandinella* reach escape speeds of 100–150 body lengths per second (Gilbert 1994; Jakobsen 2001). However, *C. simplex* and *Rhodomonas salina* (Jakobsen et al. 2006) can achieve similar relative escape speeds as dinoflagellates and ciliates with just two relatively short flagella.

Reversed swimming as an escape response is well-known in the biflagellate *Chlamydomonas reinhardtii* (Bray 2000). The flagella reversal and the change in the flagellar beat pattern and frequency characteristic of reversed swimming in *C. reinhardti* is regulated by changes in the intracellular Ca^{2+} concentration (Hyams and Borisy 1978; Pivato and Ballottari 2021). It is likely that reversed swimming in *C. simplex* is similarly regulated, given that haptonema coiling is also dependent on Ca^{2+} (Nomura et al. 2019).

Triggering fluid signal

We investigated two components of the fluid disturbance as possible triggering signals, namely the magnitude of deformation, ϵ, and the maximum deformation rate, Δ. The microfluidic channel experiments show that only the threshold value of Δ remain constant when changing the flow rate, suggesting that it is the maximum deformation rate and not the magnitude of deformation that triggers the escape response. The response of *C. simplex* to fluid disturbance appears similar to what has been reported for zooplankton (Kiørboe et al. 1999; Kiørboe and Visser 1999). The average Δ computed at the initial escape positions in the microfluidic experiment (20.1 s^{-1} [18.4–21.8]) is similar to but slightly higher than the conservative estimate from the predator experiment (13.5 s^{-1} [10.6–17.1]). Jakobsen (2002) calculated a lower response threshold for *C. simplex* exposed to the feeding current of a ciliate (8.9 s^{-1} [6.9–10.6]). These values were, however, computed from an idealized model of the flow generated by the ciliate.

It is unclear whether the fluid signal is perceived by the haptonema or by the cell body, or both. We know that mechanical stimulation of the haptonema elicits a response, but in several observations, jumps were initiated without the haptonema being disturbed. Thus, deformation of the cell body in a deforming fluid may also, as in other protists, elicit a response.

Response latency

The response latency between the onset of the stimulus (threat) and the behavioral response is a critical component of an organism's ability to successfully escape predation. Shorter response latencies will increase the effectiveness of an escape response. The ciliates *Pseudotontonia* sp. and *Tontonia* sp. have extremely short response latencies of less than 0.9 ms (Gemmell et al. 2015). The time between the stimulus (haptonema being deformed) and the initial contraction of the haptonema in *C. simplex* is also very short, between 1 and 2 ms (Supporting Information Video S2). These response times are in the lower range of those reported for copepods, 2–10 ms (Waggett and Buskey 2008). However, in *C. simplex* the response latency between the stimulus to actual fleeing away from the danger is longer, about 15 ms, due to the additional time required for coiling the haptonema and reversing the flagella (Fig. 3; Supporting Information Video S2).

Ecological significance

Rapid escape responses are found among ciliates (Jakobsen 2001; Fenchel and Hansen 2006; Gemmell et al. 2015), dinoflagellates (Jakobsen 2002; Jakobsen et al. 2006), and haptophytes, and are an effective way to reduce predation risk. Thus, ciliate species incapable of fast escapes are 2–15 times more likely to be consumed by copepods than species that exhibit rapid escapes (Broglio et al. 2001; Jakobsen 2001). Similarly, grazing rates by both the dinoflagellate *Oxyrrhis marina* and nauplii of *T. longicornis* on *C. simplex* are significantly lower than on *P. polylepis* and *P. parvum* (Lauridsen 2024), consistent with our experiments. These two other haptophytes are, however, able to harness other defenses as some strains are toxic and may kill both their competitors and their prey (Nielsen et al. 1990; Medić et al. 2022).

The presence of the long haptonema in *C. simplex* has clear trade-offs: it serves an important function in foraging (Kawachi et al. 1991; Kawachi and Inouye 1995) and it increases the clearance rate compared to haptophytes with shorter haptonema (Dölger et al. 2017; Asadzadeh et al. 2023). However, it decreases the routine swimming speed (Table 1), and increases the hydrodynamic noise produced by the swimming cell, thus increasing its detectability to flow sensing predators, such as copepods (Asadzadeh et al. 2023). The haptonema also increases the lag time of the escape response. One may argue that haptophytes with a very long haptonema, like *C. simplex*, compensate for their elevated detectability to predators by a significant escape jump capability. Nonescaping haptophytes with shorter haptonema may harness other potential defense mechanisms, like toxicity. These different adaptations to foraging and defense among haptophytes will translate to differences in distribution patterns and population abundances in nature that will depend on food availability and the predation landscape, however, in ways that are not easy to predict.

Data availability statement

All data used to draw conclusions and compute figures are in the manuscript.

References

Asadzadeh, S. S., J. H. Walther, and T. Kiørboe. 2023. Conflicting roles of flagella in planktonic protists: Propulsion, resource acquisition, and stealth. PRX Life **1**: 013002. doi:10.1103/PRXLife.1.013002

Birkhead, M., and R. N. Pienaar. 1995. The taxonomy and ultrastructure of *Chrysochromulina simplex* (Prymnesiophyceae). Phycologia **34**: 145–156. doi:10.2216/i0031-8884-34-2-145.1

Bray, D. 2000. Cell movements. Garland Science. doi:10.4324/9780203833582

Broglio, E., M. Johansson, and P. Jonsson. 2001. Trophic interaction between copepods and ciliates: Effects of prey swimming behavior on predation risk. Mar. Ecol. Prog. Ser. **220**: 179–186. doi:10.3354/meps220179

Bruno, E., C. M. Andersen Borg, and T. Kiørboe. 2012. Prey detection and prey capture in copepod nauplii. PLoS One **7**: e47906. doi:10.1371/journal.pone.0047906

Buskey, E., P. Lenz, and D. Hartline. 2002. Escape behavior of planktonic copepods in response to hydrodynamic disturbances: High speed video analysis. Mar. Ecol. Prog. Ser. **235**: 135–146. doi:10.3354/meps235135

Calbet, A., and M. R. Landry. 2004. Phytoplankton growth, microzooplankton grazing, and carbon cycling in marine systems. Limnol. Oceanogr. **49**: 51–57. doi:10.4319/lo.2004.49.1.0051

Dölger, J., L. T. Nielsen, T. Kiørboe, and A. Andersen. 2017. Swimming and feeding of mixotrophic biflagellates. Sci. Rep. **7**: 39892. doi:10.1038/srep39892

Fenchel, T. 1982. Ecology of heterotrophic microflagellates. II. Bioenergetics and growth. Mar. Ecol. Prog. Ser. **8**: 225–231.

Fenchel, T., and P. J. Hansen. 2006. Motile behaviour of the bloom-forming ciliate *Mesodinium rubrum*. Mar. Biol. Res. **2**: 33–40. doi:10.1080/17451000600571044

Gemmell, B. J., H. Jiang, and E. J. Buskey. 2015. A tale of the ciliate tail: Investigation into the adaptive significance of this sub-cellular structure. Proc. R. Soc. Lond. B Biol. Sci. **282**: 20150770. doi:10.1098/rspb.2015.0770

Gilbert, J. J. 1994. Jumping behavior in the oligotrich ciliates *Strobilidium velox* and *Halteria grandinella*, and its significance as a defense against rotifer predators. Microb. Ecol. **27**: 189–200. doi:10.1007/BF00165817

Green, J. C., D. J. Hibberd, and R. N. Pienaar. 1982. The taxonomy of *Prymnesium* (Prymnesiophyceae) including a description of a new cosmopolitan species, *P. patellifera* sp. nov., and further observations on *P. parvum* N. carter. Br. Phycol. J. **17**: 363–382. doi:10.1080/00071618200650381

Gregson, A. J., J. C. Green, and B. S. C. Leadbeater. 1993. Structure and physiology of the haptonema in *Chrysochromulina* (Prymnesiophyceae). II. Mechanisms of haptonematal coiling and the regeneration process. J. Phycol. **29**: 686–700. doi:10.1111/j.0022-3646.1993.00686.x

Hyams, J. S., and G. G. Borisy. 1978. Isolated flagellar apparatus of *Chlamydomonas*: Characterization of forward swimming and alteration of waveform and reversal of motion by calcium ions in vitro. J. Cell Sci. **33**: 235–253. doi:10.1242/jcs.33.1.235

Jakobsen, H. H. 2001. Escape response of planktonic protists to fluid mechanical signals. Mar. Ecol. Prog. Ser. **214**: 67–78. doi:10.3354/meps214067

Jakobsen, H. H. 2002. Escape of protists in predator-generated feeding currents. Aquat. Microb. Ecol. **26**: 271–281. doi:10.3354/ame026271

Jakobsen, H. H., L. Everett, and S. Strom. 2006. Hydromechanical signaling between the ciliate *Mesodinium pulex* and motile protist prey. Aquat. Microb. Ecol. **44**: 197–206. doi:10.3354/ame044197

Jalaal, M., N. Schramma, A. Dode, H. De Maleprade, C. Raufaste, and R. E. Goldstein. 2020. Stress-induced dinoflagellate bioluminescence at the single cell level. Phys. Rev. Lett. **125**: 028102. doi:10.1103/PhysRevLett.125.028102

Kawachi, M., I. Inouye, O. Maeda, and M. Chihara. 1991. The haptonema as a food-capturing device: Observations on *Chrysochromulina hirta* (Prymnesiophyceae). Phycologia **30**: 563-573. doi:10.2216/i0031-8884-30-6-563.1

Kawachi, M., and I. Inouye. 1995. Functional roles of the haptonema and the spine scales in the feeding process of *Chrysochromulina spinifera* (Fournier) Pienaar et Norris (Haptophyta = Prymnesiophyta). Phycologia **34**: 193–200. doi:10.2216/i0031-8884-34-3-193.1

Khan, S. M. M. K., M. Arikawa, G. Omura, Y. Suetomo, S. Kakuta, and T. Suzaki. 2003. Axopodial contraction in the heliozoon *Raphidiophrys contractilis* requires extracellular Ca^{2+}. Zoolog. Sci. **20**: 1367–1372. doi:10.2108/zsj.20.1367

Kiørboe, T. 2008. A mechanistic approach to plankton ecology. Princeton University Press.

Kiørboe, T., E. Saiz, and A. Visser. 1999. Hydrodynamic signal perception in the copepod *Acartia tonsa*. Mar. Ecol. Prog. Ser. **179**: 97–111. doi:10.3354/meps179097

Kiørboe, T., and A. W. Visser. 1999. Predator and prey perception in copepods due to hydromechanical signals. Mar. Ecol. Prog. Ser. **179**: 81–95. doi:10.3354/meps179081

Kiørboe, T., A. Andersen, V. J. Langlois, and H. H. Jakobsen. 2010. Unsteady motion: Escape jumps in planktonic copepods, their kinematics and energetics. J. R. Soc. Interface **7**: 1591–1602. doi:10.1098/rsif.2010.0176

Lauridsen, N. K. 2024. Predation avoidance in haptophytes. Bachelor thesis. Technical Univ. of Denmark.

Lürling, M. 2021. Grazing resistance in phytoplankton. Hydrobiologia **848**: 237–249. doi:10.1007/s10750-020-04370-3

Maldonado, E. M., and M. I. Latz. 2007. Shear-stress dependence of dinoflagellate bioluminescence. Biol. Bull. **212**: 242–249. doi:10.2307/25066606

Manton, I. 1964. Further observations on the fine structure of the haptonema in prymnesium parvum. Arch. Mikrobiol. **49**: 315–330. doi:10.1007/BF00406854

Manton, I. 1967. Further observations on the fine structure of *Chrysochromulina chiton* with special reference to the haptonema, "peculiar" golgi structure and scale production. J. Cell Sci. **2**: 265–272. doi:10.1242/jcs.2.2.265

Manton, I., and M. Parke. 1962. Preliminary observations on scales and their mode of origin in *Chrysochromulina polylepis* sp. nov. J. Mar. Biol. Assoc. UK **42**: 565–578. doi:10.1017/S0025315400054266

Medić, N., E. Varga, D. B. Van de Waal, T. O. Larsen, and P. J. Hansen. 2022. The coupling between irradiance, growth, photosynthesis and prymnesin cell quota and production in two strains of the bloom-forming haptophyte, *Prymnesium parvum*. Harmful Algae **112**: 102173. doi:10.1016/j.hal.2022.102173

Nielsen, T. G., T. Kiørboe, and P. K. Bjørnsen. 1990. Effects of a *Chrysochromulina polylepis* subsurface bloom on the planktonic community. Mar. Ecol. Prog. Ser. **62**: 21–35. doi:10.3354/meps062021

Nielsen, L. T., and T. Kiørboe. 2021. Foraging trade-offs, flagellar arrangements, and flow architecture of planktonic protists. Proc. Natl. Acad. Sci. USA **118**: e2009930118. doi:10.1073/pnas.2009930118/-/DCSupplemental

Nomura, M., K. Atsuji, K. Hirose, K. Shiba, R. Yanase, T. Nakayama, K. Ishida, and K. Inaba. 2019. Microtubule stabilizer reveals requirement of Ca^{2+}-dependent conformational changes of microtubules for rapid coiling of haptonema in haptophyte algae. Biol. Open **8**(2): bio036590. doi:10.1242/bio.036590

Ockleford, C. D., and J. B. Tucker. 1973. Growth, breakdown, repair, and rapid contraction of microtubular axopodia in the heliozoan Actinophrys sol. J. Ultrastruct. Res. **44**: 369–387. doi:10.1016/S0022-5320(73)90005-1

Pančić, M., and T. Kiørboe. 2018. Phytoplankton defence mechanisms: Traits and trade-offs. Biol. Rev. **93**: 1269–1303. doi:10.1111/brv.12395

Pivato, M., and M. Ballottari. 2021. *Chlamydomonas reinhardtii* cellular compartments and their contribution to intracellular calcium signalling. J. Exp. Bot. **72**: 5312–5335. doi:10.1093/jxb/erab212

Polin, M., I. Tuval, K. Drescher, J. P. Gollub, and R. E. Goldstein. 2009. *Chlamydomonas* swims with two "gears" in a eukaryotic version of run-and-tumble locomotion. Science **325**: 487–490. doi:10.1126/science.1172667

Ryu, S., M. J. Lang, and P. Matsudaira. 2012. Maximal force characteristics of the Ca^{2+}-powered actuator of *Vorticella convallaria*. Biophys. J. **103**: 860–867. doi:10.1016/j.bpj.2012.07.038

Shen, X., Marcos, and H. C. Fu. 2020. How the bending mechanics of setae modulate hydrodynamic sensing in copepods. Limnol. Oceanogr. **65**: 749–761. doi:10.1002/lno.11344

Shen, X., X. Yao, Marcos, and H. C. Fu. 2021. Can the mechanoreceptional setae of a feeding-current feeding copepod detect hydrodynamic disturbance induced by entrained free-floating prey? Limnol. Oceanogr. **66**: 4096–4111. doi:10.1002/lno.11945

Suzaki, T., Y. Shigenaka, S. Watanabe, and A. Toyohara. 1980. Food capture and ingestion in the large heliozoan, *Echinosphaerium nucleofilum*. J. Cell Sci. **42**: 61–79. doi:10.1242/jcs.42.1.61

Suzaki, T., M. Ando, K. Ishigame, Y. Shigenaka, and M. Sugiyama. 1992. Structure and function of the cytoskeleton in heliozoa. Eur. J. Protistol. **28**: 430–433. doi:10.1016/S0932-4739(11)80007-6

Waggett, R. J., and E. J. Buskey. 2008. Escape reaction performance of myelinated and non-myelinated calanoid copepods. J. Exp. Mar. Biol. Ecol. **361**: 111–118. doi:10.1016/j.jembe.2008.05.006

Wan, K. Y., K. C. Leptos, and R. E. Goldstein. 2014. Lag, lock, sync, slip: The many "phases" of coupled flagella. J. R. Soc. Interface **11**: 20131160. doi:10.1098/rsif.2013.1160

Acknowledgments

We are grateful to Erika Causa and Pietro Cicuta for generously providing facilities and training for production of the microfluidic channels at the University of Cambridge. Furthermore, we are grateful to Niels Daugbjerg for supplying the haptophyte cultures, Massimiliano Rossi for helping with the pump and microfluidic setup, and Jack Melbye for taking care of the copepod cultures. We received funding from The Independent Research Fund Denmark (7014-00033b), the Carlsberg Foundation (CF17-0495), the Simons Foundation (931976), and the European

Union's Horizon 2020 research and innovation program under Marie Skłodowska-Curie grant agreement no. 955910. The Centre for Ocean Life is supported by the Villum Foundation.

Conflict of Interest

None declared.

Submitted 30 April 2024
Revised 16 August 2024
Accepted 22 September 2024

Associate editor: Miriam Gerhard